

RE J1034+396: The origin of the soft X-ray excess and QPO

Matthew Middleton¹, Chris Done¹, Martin Ward¹, Marek Gierliński¹ and Nick Schurch¹

¹Department of Physics, University of Durham, South Road, Durham DH1 3LE, UK

31 October 2018

ABSTRACT

The X-ray quasi-periodic oscillation (QPO) seen in RE J1034+396 is so far unique amongst AGN. Here we look at the another unique feature of RE J1034+396, namely its huge soft X-ray excess, to see if this is related in any way to the detection of the QPO. We show that all potential models considered for the soft energy excess can fit the 0.3–10 keV X-ray spectrum, but that the energy dependence of the rapid variability (which is dominated by the QPO) strongly supports a spectral decomposition where the soft excess is from low temperature Comptonization of the disc emission and remains mostly constant, while the rapid variability is produced by the power law tail changing in normalization. The presence of the QPO in the tail rather than in the disc is a common feature in black hole binaries, but low temperature Comptonization of the disc spectrum is not generally seen in these systems. The main exception to this is GRS 1915+105, the only black hole binary which routinely shows super-Eddington luminosities. We speculate that super-Eddington accretion rates lead to a change in disc structure, and that this also triggers the X-ray QPO.

Key words: accretion, accretion discs – galaxies: active – X-rays: galaxies

1 INTRODUCTION

The discovery of a significant quasi-periodic oscillation in the X-ray light curve of a Narrow Line Seyfert 1 AGN RE J1034+396 (Gierliński et al. 2008) strengthens arguments stressing the similarities in the physics of the accretion flow between supermassive and stellar mass black holes. Previous evidence for a simple correspondence between AGN and the black hole binaries (BHB) included similarities in the broadband shape of the X-ray variability power spectra, with characteristic break timescales scaling with mass (e.g. M°Hardy et al. 2006), but the characteristic QPOs often seen in BHB light curves remained undetected until now (Vaughan & Uttley 2005; Leighly 2005).

The QPOs in BHB can be split into two main groups, at high and low frequencies, respectively. While there is as yet no clear mechanism for producing either set of QPOs (or the correlated broad band variability) there are many pointers to their origin from the observations. Most clearly, their amplitude increases with increasing energy. The BHB spectra typically contain two components, a disc and tail, and this increasing amplitude is consistent with the QPO (and all the rest of the rapid variability) being associated with a variable tail while the disc remains constant. This shows that QPOs are produced by some mode of the hot coronal flow rather than a mode of the thin disc. (see e.g. the reviews by Van der Klis 2004; McClintock & Remillard 2006; Done, Gierliński & Kubota 2007).

The rest of the QPO properties are more complex. The high frequency (HF) QPO may have a constant fundamental frequency

(though it is seen at 3:2 harmonic ratios of this), which may relate to the mass of the black hole. By contrast, the frequency (and other properties) of the low frequency (LF) QPO change dramatically with mass accretion rate, correlating with the equally dramatic changes in the source spectra. Typically these show that at low mass accretion rates compared to Eddington, $L/L_{\text{Edd}} \ll 1$, the LF QPO is at low frequencies, but is weak and rather broad. The corresponding energy spectra are dominated by a hard power law (photon index $\Gamma < 2$) which rolls over at around 100 keV (low/hard spectral state). As the mass accretion rate increases, the low frequency QPO increases in strength and coherence as well as frequency, while the power law spectrum softens and the disc increases in strength relative to the power law. The QPO is at its highest frequencies, is strongest and most coherent where the spectrum has both a strong disc component and a strong soft tail of emission to higher energies ($\Gamma > 2.5$). After this, the LF QPO frequency remains more or less constant as the tail declines and hardens to $\Gamma \sim 2.2$, leaving the spectra dominated by the disc component (high/soft state), though it becomes harder to follow the QPO as increasing contribution from the stable disc (thermal dominant state) swamps the signal from the variable tail. (e.g. McClintock & Remillard 2006 and references therein)

The only major difference expected in scaling these models up to the supermassive black holes in AGN is the decrease in disc temperature down to the UV band. The X-ray spectra of AGN spectra should then be always dominated by the tail, irrespective of spectral state (e.g. Done & Gierliński 2005). The predicted change in shape of the tail with spectral state/mass accretion rate gives an ex-

planation for the variety of spectral properties seen in *unobscured* subtypes AGN such as Broad Line AGN, Narrow Line Seyfert 1's (NLS1) and LINERs (e.g. Middleton et al. 2008). The generally hard X-ray spectra seen in LINERs could be explained as a low L/L_{Edd} flow (e.g. Yuan et al. 2008 but see Maoz 2007), while broad line AGN with a strong UV disc component and weak X-ray $\Gamma \sim 2$ tail would be analogous to the high/soft state in BHB. The NLS1 probably have the highest mass accretion rates, so have lower mass for a given luminosity (Boroson 2002), and their steeper X-ray spectra (Brandt, Mathur & Elvis 1997; Leighly 1999; Shemmer et al. 2006) make them natural counterparts for the very high state (Pounds, Done & Osborne 1995; Murashima et al. 2005; Middleton et al. 2007, M^cHardy et al. 2007) where all QPOs (both high and low frequencies) are strongest. Intriguingly, RE J1034+396 is a NLS1, so its QPO detection is consistent with these scaling models.

All this supports models where the underlying physics of the accretion flow is very similar between BHB and AGN. However, the scaling clearly breaks down under more detailed study of the X-ray spectra from high mass accretion rate objects. These should have spectra dominated by the steep tail which is typical of the high and very high states, with no disc emission in the X-ray band. Yet *all* the high mass accretion rate AGN show an excess below 1 keV (Gierliński & Done 2004; Brocksopp et al. 2006). This 'soft X-ray excess' is completely inconsistent with the expected disc component, both as its temperature is higher than predicted from the mass and mass accretion rate of these AGN (e.g. Bechtold et al. 1987), and as its shape is much smoother than a sharply peaked disc spectrum (Czerny et al. 2003; Gierliński & Done 2004). Either the soft X-ray excess is an additional component which breaks the scaling between AGN and BHB, or it is produced by some external distortion of the intrinsic emission. Obviously it is very important to distinguish between these alternatives and the objects with the strongest soft excesses offer the most stringent constraints.

RE J1034+396 has one of the largest soft excesses known, which appears to connect smoothly onto the enormous EUV peak of its spectral energy distribution (Middleton et al. 2007). The size and temperature of this peak is extreme even amongst NLS1's (Puchnarewicz et al. 2002, Casebeer et al. 2006; Middleton et al. 2007), and an obvious question is whether this extreme soft excess is somehow linked to the detection of the QPO. Here we use XMM-Newton data on RE J1034+396 to test the various models for the soft X-ray excess, and speculate on its connection to the QPO.

2 THE ORIGIN OF THE SOFT EXCESS IN HIGH MASS ACCRETION RATE AGN

There are multiple models for the origin of the soft X-ray excess seen ubiquitously in high mass accretion rate AGN. The most obvious possibility is that it is related somehow to the disc. One way to do this is if the mass accretion rate is super Eddington, so the disc spectrum is distorted by advection of radiation in the very optically thick flow. Such slim discs (Abramowicz et al. 1988) have spectra which are less peaked than a standard disc (Watarai et al. 2000) so give a better fit to the shape of the soft excess (Mineshige et al. 2000; Wang & Netzer 2003; Haba et al. 2008). Another way to modify the shape of the (standard or slim) disc emission is if it is Comptonized by low temperature electrons (Czerny & Elvis 1987; Kawaguchi 2003), perhaps produced by a hotter skin forming over the cooler disc (Czerny et al. 2003). However, the derived temperature for this skin is remarkably similar for all objects at 0.1–0.2 keV despite a large range in black hole mass (and hence disc

temperature: Czerny et al. 2003; Gierliński & Done 2004, Crummy et al. 2006). This argues against it being related to the disc, so it is unlikely to be a true continuum component.

Instead, a constant energy is most easily explained through atomic processes, in particular the abrupt increase in opacity in partially ionized material between ~ 0.7 –2 keV due to OVII/OVIII and Fe transitions. This results in an increase in transmitted flux below 0.7 keV, which could produce the soft excess either from absorption in optically thin material in the line of sight, or from reflection by optically thick material out of the line of sight. In both models the observed smoothness of the soft excess requires large velocity smearing (velocity dispersion $\gtrsim 0.3$ c) in order to hide the characteristic *sharp* atomic features, but with this addition then both reflection and absorption models fit the shape of the soft excess equally well (Fabian et al. 2002, 2004; GD04; Crummy et al. 2006; Chevallier et al. 2006; Schurch & Done 2006; Middleton et al. 2007; Dewangan et al. 2007, D'Ammando et al. 2008). Such high velocities are naturally produced only close to the black hole, so both absorption and reflection models predict that the soft excess arises in regions of strong gravity. However, both models also require some extreme, and probably unphysical, parameters. In the reflection model, the inferred smearing can be so large that the required emissivity must be more strongly centrally peaked than expected from purely gravitational energy release, perhaps pointing to extraction of the spin energy itself. The amount of reflection required to produce the soft excess can also be extreme. Quasi- isotropic emission sets a limit to size of the soft excess of no more than a factor of 2–3 above the harder continuum emission (Sobolewska & Done 2007), yet the strongest observed soft excesses are a factor 4 larger than this (a factor 8–10 above the extrapolated continuum), requiring that the intrinsic illuminating spectrum is strongly suppressed (e.g. Fabian et al. 2002). This issue becomes even more problematic when incorporating any pressure balance condition (such as hydrostatic equilibrium) as this strongly limits the section of the disc in which partially ionized material can exist, hence makes a much smaller soft excess (Done & Nayakshin 2007; Malzac, Dumont & Mouchet 2005).

Conversely, in the smeared absorption model, pressure balance rather naturally produces the required partially ionized zone (Chevallier et al. 2006). However, these models also imply extreme velocities, with a peak outflow velocity of ~ 0.8 c required in order to smooth away the characteristic absorption features from a smooth wind which covers the source (Schurch & Done 2007, 2008). This is much larger than the maximum velocity of ~ 0.2 –0.4c produced by models of a radiation driven disc wind (Fukue 1996), so the absorber must instead be associated with faster material in this description. The obvious physical component would be a jet/magnetic wind, yet the amount of material is probably far too large to be associated with either of these (Schurch & Done 2007; 2008).

Thus there are physical problems with all of these models: the Comptonized disc cannot explain the narrow range in inferred temperatures, smeared reflection cannot produce the strongest soft excesses seen if the disc is in hydrostatic equilibrium, and smeared absorption requires a fast wind/jet which is not readily associated with the properties of any known component.

An alternative possibility for the absorption model is that the characteristic absorption features are masked by dilution instead of smearing, perhaps due to the wind becoming clumpy so that it partially covers the source (Boller et al. 1996; Tanaka et al. 2004; Miller et al. 2007; 2008). These models lack diagnostic power as the potential complexity of the wind means that any number of par-

tial absorbers can be added until the model fits the observed spectra. Nonetheless, this may correspond to the more messy reality of high Eddington fraction winds from UV luminous discs (Proga & Kallman 2004). Some of the clumps could even have high enough column to produce significant reflected emission as well (Malzac et al. 2005; Chevallier et al. 2006), giving a complex mix of reflection and partial absorption from a range of different columns, velocities and ionization states of the material.

It is important to distinguish between these very different potential origins of the soft excess as they make very different predictions about the environment and geometry of the accreting material close to the black hole. The extreme broad iron lines required in the pure reflection models are not required in the absorption models (either smeared: Sobolewska & Done 2007; Done 2007 or partial covering: Miller et al. 2008) as the broad feature redwards of the iron line is fit instead by continuum curvature. All the absorption models require the presence of material above the inner disc, probably in the form of a wind, whereas the reflection models instead suggest a clean line of sight to the inner disc. The large velocity shear in the smeared wind model requires that the material is strongly accelerated, so it potentially carries an enormous amount of kinetic energy (Chevallier et al. 2006; Schurch & Done 2006) with corresponding impact on AGN feedback/galaxy formation.

Spectral fitting alone cannot distinguish between these very different spectral models in the 0.3–10 keV bandpass (Crummey et al. 2007; Sobolewska & Done 2007; Middleton et al. 2007; Miller et al. 2007; 2008). Variability gives additional information, but the smeared reflection and smeared absorption models are known to be able to predict similar variability patterns (Ponti et al. 2005; Gierliński & Done 2006). Here for the first time we fit *all* of these models to the data and calculate their predicted variability to see which description of the soft excess best matches the *simultaneous* constraints from both spectral and variability data.

3 DATA EXTRACTION

XMM-Newton observed RE J1034+396 on 2007-05-31 and 2007-06-01 for about 93 ks (observation id. 0506440101, revolution no. 1369). We extracted source and background light curves and noticed background flares and data gaps in the final 7 ks. Therefore, we excluded this data segment from analysis and used 84.3 ks of clean data starting on 2007-05-31 20:10:12 UTC for further analysis.

3.1 Spectra

We selected data from the PN (patterns 0–4) and MOS (patterns 0–12) in a region of radius 45 arcsec. The data are very similar in shape to a previous 16 ks *XMM-Newton* observation, but are much higher quality due to the longer exposure. Because of the extreme softness of this particular source both MOS and PN were piled up so we excised the central regions of the image out to 7.5 arcsec radius so as not to be affected by this. Background was taken from 6 source free regions of the same size.

We use only the MOS data in the 0.3–10 keV range for spectral fitting as there are well known discrepancies at soft energies between the PN and MOS spectra which makes simultaneous fitting of these two instruments very difficult.

We use XSPEC version 11.3.2, and fix the minimum galactic absorption at $1.31 \times 10^{20} \text{ cm}^{-2}$ in all fits, but also allow a separate

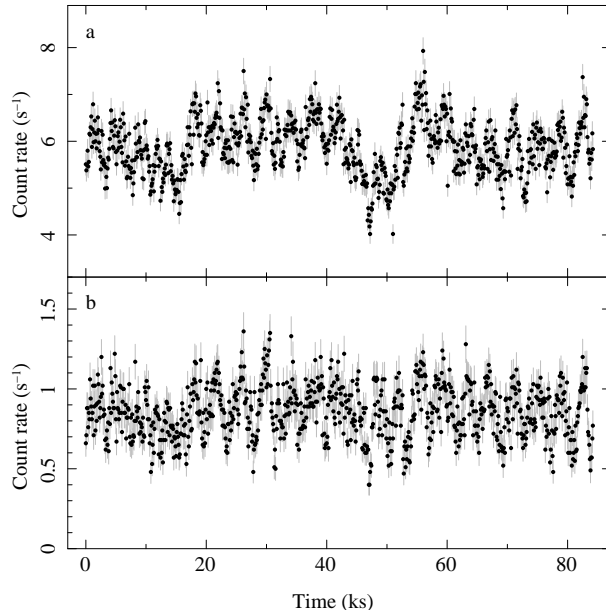


Figure 1. Light curve of *XMM-Newton* (all detectors added together) observation of RE J1034+396 in (a) 0.3–10 and (b) 1–10 keV band. Clearly the ‘dip’ occurring ~ 50 ks into the observation has little effect upon the light curve at high energies. The starting time of this observation was 2007-05-31 20:10:12 UTC.

neutral absorption column to account for additional absorption in the host galaxy.

3.2 Energy dependence of the variability: rms spectra

A successful model must be able to describe *both* the spectrum *and* the variability. Fig. 1a shows the full light curve for these data, with the clear QPO which is remarkably coherent in the latter part of the observation (25–85 ks: G08). There is also a large scale drop in flux at 40–55 ks. This looks very similar to an occultation event such as those recently recognised in other AGN (McKernan & Yaqoob 1998; Gallo et al. 2004; Risaliti et al. 2007; Turner et al. 2008). Fig. 1b shows the light curve in the high energy bandpass, where this dip is *not* present. This shows that there is clearly energy dependent variability in this event which is not present in the rest of the light curve. Thus the variability is *complex* and made from more than one component.

We explore this further by calculating the root mean square fractional variability amplitude (hereafter we will use the term ‘rms’ for simplicity) as a function of energy (see Edelson et al. 2002; Markowitz, Edelson & Vaughan 2003 and Vaughan et al. 2003). We first calculate this for the total light curve with 100-s binning. Fig. 2a shows this rms spectrum rising smoothly with energy. This behaviour is quite unlike the rms spectra seen from other NLS1’s although these can show a variety of shapes, including flat (e.g. Gallo et al. 2007; O’Neill et al. 2007), flat with a peak at 2 keV (Vaughan & Fabian 2004; Gallo et al. 2004; Gallo et al. 2007), and falling but with a peak at 2 keV (Ponti et al. 2006; Gallo et al. 2007; Larsson et al. 2008).

The rms is dominated by noise above ~ 4 keV as the count rate at high energies is very low due to the steep spectrum. In order to extend the rms to higher energies we extract light curves from the full source region, without excising the core to correct for pileup

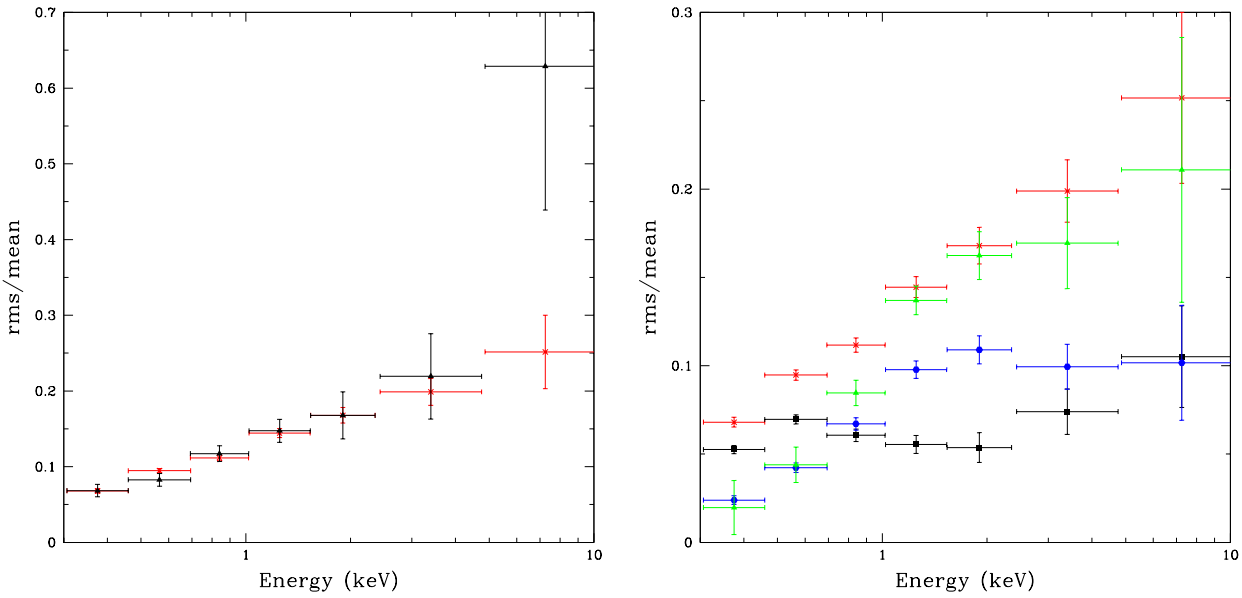


Figure 2. Rms spectra. Panel (a) shows the rms from the data with the PSF core excised (black triangles). The rms rises linearly with energy but the uncertainties at high energies are large due to the low number of counts. Better statistics at high energy can be obtained by including all the data (red crosses). Pileup transfers photons from low energy to high energy, but the lack of variability in the data at low energy means that this effect dilutes the high energy rms. Thus these data give a lower limit on the variability at high energies. Panel (b) shows the different rms patterns produced from different timescale variability using all the data. The red crosses show the total variability as in (a), while the black squares show the long timescale variability (11.2–5000 μ Hz), the blue circles show the rms of the QPO alone (frequency of 270 μ Hz) and the green triangles show the rms of the rapid variability, including the QPO (135–5000 μ Hz).

(red points in Fig. 2b). This means that some fraction of the hard photons originate from much lower energies, but the steeply rising rms spectrum means that the variability of these pileup photons is rather small. Thus pileup adds an approximately constant offset to the hard spectrum, and so should dilute the variability seen at high energies. Instead, the rms spectrum continues to rise in a rather smooth fashion at high energies (red points in Fig. 2b), showing that this is a good lower limit to the total variability at high energies.

The smooth increase of the rms as a function of energy seems initially most likely to be from a single component. However, there is clear evidence of different processes contributing to the variability from the different energy dependence seen in the dip event (Fig. 1). We explore this by re-calculating the rms on a range of timescales by changing the bin time, ΔT , of the light curves. The rms is the square root of the integrated power in the light curve from frequencies of $1/T$ to $1/(2\Delta T)$ Hz, where $T = 84300$ s is the length of the light curve. Thus the original binning of 100 s means that the rms at each energy is the integral of the power spectrum from 11.2 to 5000 μ Hz. We compare this to the rms of the long timescale variability by increasing the binning to 3700 s (the QPO period), i.e. corresponding to the frequency range 11.2–135 μ Hz. This is shown by the black data in Fig. 2b, and has a very different shape to the total rms (red points), with a similar amount of variability at low energies, but a sharp break around 0.7 keV so that the variability at high energies is much lower. Subtracting this long timescale rms from the total rms (in quadrature) gives the rms of the rapid variability (including the QPO at 270 μ Hz), i.e. the integral of the power spectrum from 135 to 5000 μ Hz (green points in Fig. 2b). This has a sharp rise with increasing energy at low energies. We can compare this directly to the rms of the QPO by calculating this from the folded light curve (blue points). This is indeed very similar in shape and normalization to the rms of rapid variability. This is expected as the QPO forms a large fraction (more than half) of

the variability power in this frequency range. However, the shape at high energies is marginally different, with the rapid variability appearing to continue rising with energy while the QPO saturates at an rms of ~ 0.2 . Given the potential problems with pileup, and the size of the uncertainties, this difference is probably not significant.

4 SIMULTANEOUS CONSTRAINTS FROM SPECTRA AND VARIABILITY

In the following sections we take each model for the soft excess and fit it to the 0.3–10 keV spectrum. The models are listed in Table 1. The fit results are shown in Table 2. Then we inspect this best-fitting model to see how varying these components might produce the observed energy dependence of the variability. We focus here on the rapid variability, which is dominated by the QPO, as it is clear that the longer timescale variability may contain contributions from multiple processes. We calculate the simulated rms spectra by randomly varying a spectral model parameter with the mean equal to the best-fitting value and a certain standard deviation (Gierliński & Zdziarski 2005). We calculate the rms spectrum at high energy resolution, but then bin this to the same resolution as the rms for direct comparison.

4.1 Separate component for the soft excess: DISK, SLIM and COMP

We first test the models where the soft excess is a separate emission component. A standard accretion disc spectrum (DISKBB in XSPEC) is much more strongly peaked than the data, giving a very poor fit, $\chi^2_\nu = 517/211$, showing that this is an unacceptable description of the broad band curvature. Instead we test models of an advective (slim) disc, however the best estimates for mass give a

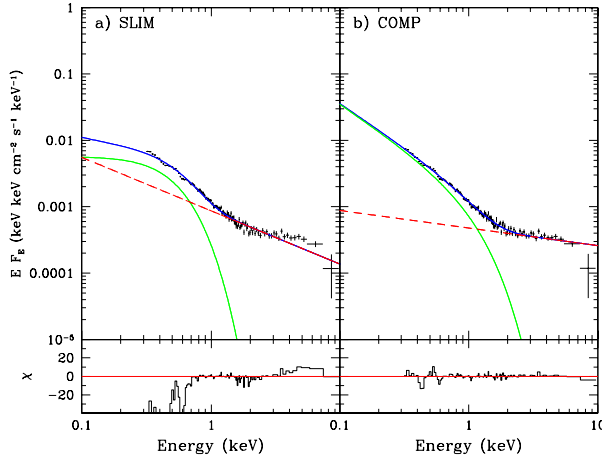


Figure 3. Spectral models for a separate component for the soft excess: The upper panel shows the deconvolved spectra, while the lower panel shows residuals to the fit. (a) uses an advective disc to describe the soft excess while (b) uses a Comptonized disc (green solid curve). Both models require a separate power law to fit the spectrum above 2 keV (red dashed line) to produce the total spectrum (blue solid line). The lower panel shows the residuals to the model fit. It is clear that the smooth curvature of the soft excess rules out the simple advective disc model, while it is well described by the Comptonized disc.

mass accretion rate of $\sim 0.3L_{\text{Edd}}$, not formally high enough for advection to be important. Theoretical calculations show that the spectrum of a slim disc can be approximated by sum of blackbodies, similar to the standard disc models, but with $T \propto r^{-p}$, where $0.5 < p < 0.75$ (the higher limit is the standard disc profile, while the lower limit is a fully advection dominated disc: Waterai et al. 2000). Fig. 3a shows that such models (DISKPBB, available as an additional local model for XSPEC) are still not broad enough to match the shape of the soft excess ($\chi^2_{\nu} = 457/210$). Instead, a low temperature Comptonization component (COMPTT) gives a reasonable fit to the data, except for the features below ~ 0.6 keV (Fig. 3b). Hereafter we refer to this model as COMP.

It is plain from the residuals to this fit (lower panel of Fig 3b) that there are weak atomic features at low energies, especially at ~ 0.6 keV. Adding a series of narrow Gaussians gives a reduction in χ^2 of ~ 30 for significant emission features at $\sim 0.55, 0.74$ and 0.87 keV. These are consistent with He-like O Ly α and He- and H-like O radiative recombination continua i.e. indicating photoionized material. However, there are no corresponding narrow lines in the RGS data, so these features must be intrinsically broad. Their equivalent width is ≤ 10 eV, so these have negligible impact on the derived continuum which is the subject of this paper.

In BHB the power law tail is generically very variable, while the disc is remarkably constant (Churazov et al. 2000). If the soft excess is really related to the disc and is constant, then we expect the low energy variability to be suppressed, as observed, because of increasing dilution of the variable power law by the constant soft excess at low energies.

We quantify this effect by taking the same Comptonization plus power law model as fits the spectrum of the soft excess, and

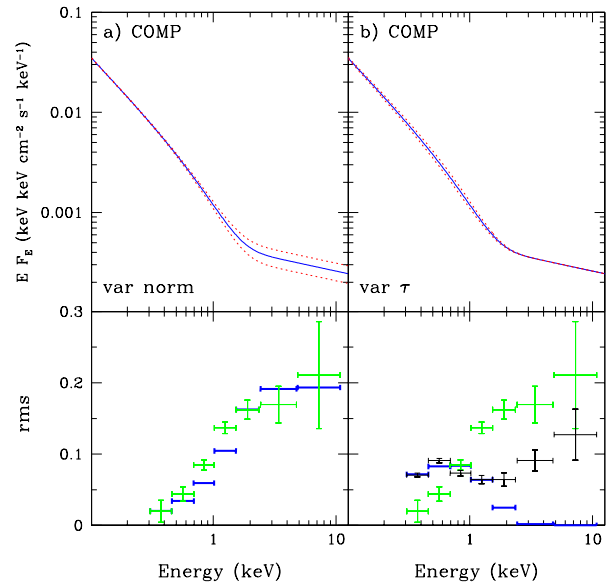


Figure 4. Variability of a Comptonized disc and power law: The upper panel shows the mean spectrum (solid blue curve) and $\pm 1\sigma$ variability (dotted red curves). The lower panel shows the rms produced by this variability (dark thick blue horizontal lines) compared to that seen in the data on short (light green crosses) and long (black crosses) timescales. Panel (a) shows the patterns produced by varying the power law in normalization while keeping the Comptonized disc constant. The rapid increase in dilution of the power law variability below 1 keV exactly matches the rapid drop on short timescales. This is very strong evidence that this spectral decomposition is correct. (b) shows the pattern produced by changing the optical depth of the Comptonized disc by 1.5 per cent, whilst keeping the power law constant. This gives a fairly good match to the observed long timescale variability (shown as black crosses in the lower panel).

varying the normalization of the power law tail by 20 per cent. This gives a constant rms where the tail dominates (above 2 keV) and a dramatically increasing suppression of the variability below this, as the fractional contribution of the constant soft excess increases (Fig. 4a). This looks very similar to the drop observed at low energies in rms of the rapid variability (and QPO). This provides very strong evidence that a two component model is the correct spectral decomposition as both the spectrum and spectral variability can be easily described in this model. The soft excess is a separate component above the power-law tail at low energies, and the rapid variability (including the QPO) is a modulation of the tail.

The longer timescale variability can also be fit in this model. The data show a rise in rms with energy to ~ 1 keV so this cannot be produced by simply varying the norm of the Comptonized disc. Instead, varying the optical depth or temperature leads to spectral pivoting about the peak of the seed photons (at $\sim 3kT_{\text{seed}} \approx 0.15$ keV). Fig. 4b shows how changing the optical depth by 1.5 per cent can produce this characteristic rise, which is then diluted by the constant power law above ~ 0.8 keV. While this does indeed match the broad shape of the long timescale rms, we caution that there should also be some contribution to this from partial covering if the dip in the light curve is indeed an occultation event.

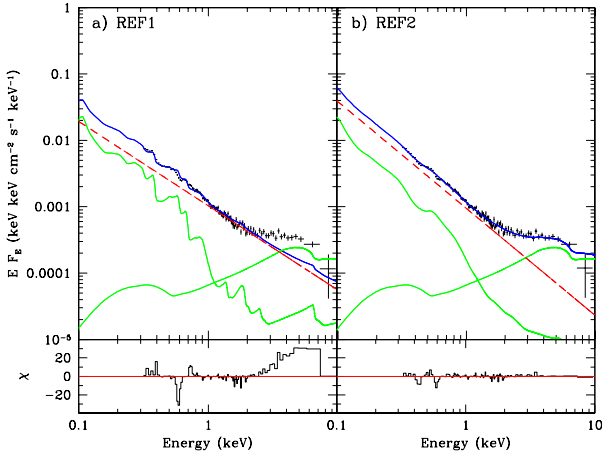


Figure 5. As for Fig. 3 but for a reflection origin for the soft excess. (a) has a steep power law (red dashed line) and its ionized, smeared reflection (light green curve) while (b) has the steep power law illuminating two separate reflectors, one of which is similarly ionized to that in (a) and one which is predominantly neutral. The residuals clearly show that at least two reflectors are required to describe the spectrum in this model.

4.2 Smeared Reflection models: REF1 and REF2

We next explore how the reflection model for the soft excess can fit both the spectrum and spectral variability. We use the constant density reflection models of Ballantyne, Iwasawa & Fabian (2001) (available as a table model in XSPEC). These models (described in more detail in Ross & Fabian 2002) become inaccurate for $\Gamma > 2.5$ (Done & Nayakshin 2007), so instead we use the spectra tabulated for $\Gamma = 2.2$, and multiply the model by $E^{-(\Gamma-2.2)}$, where E is energy. This code also converts the normalization of the reflected emission to that of the illuminating power law so that the amount of reflection is parameterized by the solid angle of the illuminated material, $\Omega/2\pi$ and inclination (Done & Gierliński 2006), which we fix at 30° . We smear this using the convolution version of the LAOR code for the velocity structure of an extreme Kerr spacetime (Laor 1991).

Fig. 5a shows that this is a very poor fit to the data ($\chi^2_\nu = 612/210$), as a single ionization state reflector cannot simultaneously produce both the hard tail *and* the shape of the soft excess. This is a common feature in good signal-to-noise data: multiple reflectors are required, one to fit the soft excess, another to fit the iron line, dispelling a key attraction of the model (Crummey et al. 2006). Nonetheless, a double reflector can indeed fit the data well (Fig. 5b), where the hard tail/iron line region requires a neutral reflector (modelled using the THCOMP code: Źycki, Done & Smith 2000 as the REFLION code does not extend down to the very low ionization states required). We hereafter refer to this model as REF2.

This is a very different spectral deconvolution to the one where the soft excess is a separate Comptonized component (COMP). The spectrum at low energies is now modelled by the intrinsic power law, and instead there is a ‘hard excess’ at high energies which is

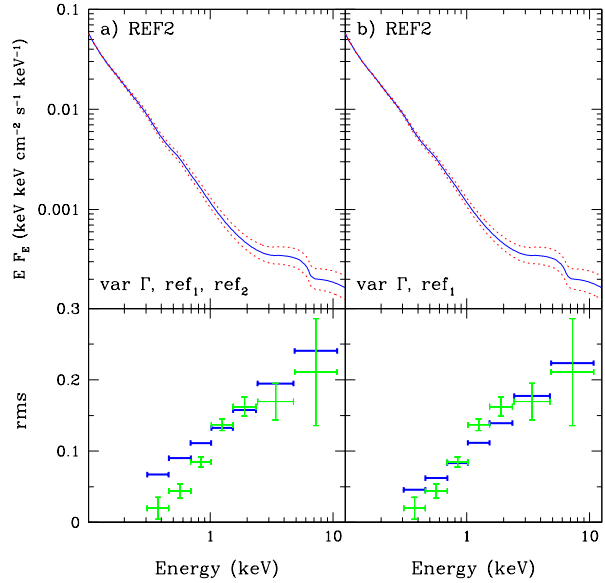


Figure 6. As for Fig. 4 but for the double reflection model for the soft excess. (a) shows the rms produced by pivoting the illuminating power law spectral index about the peak in seed photon flux at $3kT_{\text{seed}} \sim 0.15$ keV when both reflectors respond to this illumination. This gives a linear rise in rms as a function of energy, which does not match the sharper rise around 0.8 keV seen in the rapid variability. (b) shows that this can be roughly matched if the ionized reflector which contributes mainly at low energies remains constant while the more neutral reflector responds to the power law pivoting.

formed by dramatically enhanced, strongly smeared, neutral reflection.

The only way to produce a steeply rising rms is to pivot the power law about its peak in seed photons (around 0.15 keV, as before). This gives a linearly rising rms as shown in Fig. 6a, assuming both reflectors respond to this changing illumination (though we fix the ionization of each component for simplicity).

While this would fit the overall rms shown in Fig. 2b, it plainly cannot match the two very different shaped components which underlie the variability. The rapid variability rms shape does *not* rise linearly with energy, there is a clear inflection point around ~ 0.8 keV. This has an obvious origin in the separate Comptonized disc models discussed above, as this is the energy at which this component starts to dominate the spectrum and hence dilute the variability. However, it is possible to match this in the reflection model by assuming that the ionized reflector remains constant. Fig. 6b shows how this dilutes the variability towards lower energies, giving a fairly good fit to the rapid variability rms.

Constant reflection components are a feature of these models for the soft excess in other AGN, and may arise from strong light bending effects (Miniutti & Fabian 2004). This simultaneously explains the lack of variability together with enhanced amplitude and extreme smearing. However, our spectral deconvolution and variability require that the constant reflector is the one which is *not* enhanced relative to the illuminating power law, making this model appear somewhat contrived in RE J1034+396.

4.3 Smeared Absorption Models: SWIND and XSCORT

We now fit the smeared absorption models. These assume the source is completely covered by a partially ionized wind from

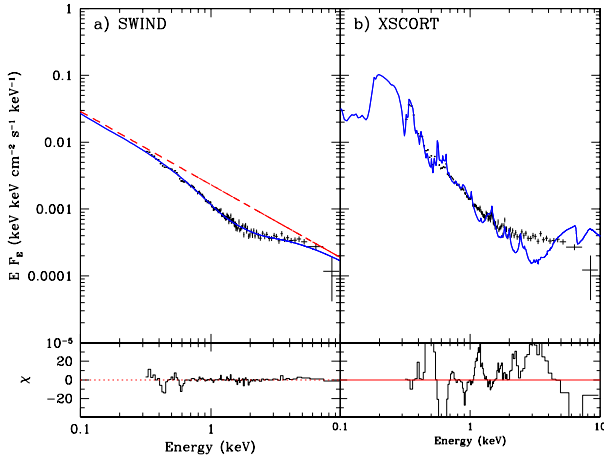


Figure 7. As for Fig. 3 but for a smeared absorption origin for the soft excess. (a) has a steep power law (dashed red line) which is distorted by a velocity smeared absorber which completely covers the source (solid blue curve). This produces a very good fit to the spectrum, but requires a large velocity dispersion in the material. (b) shows instead the results using the expected velocity dispersion from a line driven disc wind. The velocity spread of 0–0.3c is not sufficient to smear out the characteristic atomic features.

the disc, which has a large velocity shear to smear out the characteristic strong absorption lines. We first use the simple SWIND model (available on the local models page for XSPEC) of Done & Gierliński (2004; 2006), where the absorption from a partially ionized column of material is convolved with a Gaussian velocity field. This is an excellent fit to the data (Fig. 7a), but the best fit velocity dispersion goes to the upper limit of 0.5c allowed in the model. The gaussian form of the velocity dispersion means that this corresponds to a velocity shear greater than the speed of light, which is obviously unphysical (see Middleton et al. 2007, Schurch & Done 2007a, b).

Instead we fit more physical wind absorption models, calculated from the XSCORT code, which accelerate the wind from 0 to 0.3c, and use this internal velocity field self-consistently in the photoionization code. These models have only been calculated for a small number of parameters (Schurch & Done 2007a), so cannot be properly fit to the data. However, we have taken the model with parameters closest to those required by the soft excess spectral shape, and then corrected for the different spectral index, as in Section 4.2. Fig. 7b shows that while this gives a strong soft excess, the velocity shear is insufficient to smooth the strong atomic features in the 0.7–3 keV band into the observed smooth rise, so this gives a very poor fit to the data ($\chi^2_\nu = 2153/212$). Thus the absorption does not arise in a line driven disc wind, but instead must be connected to much faster moving material in this model.

We explore the variability properties of the fast wind Fig. 7a, since the more physical wind (Fig. 7b) does not fit the data. Because the whole spectrum is again made from the intrinsically steep power law, then simply pivoting this at the peak flux of the seed photons gives a linearly rising rms (Fig. 8a), similar to that of Fig. 6a. Instead, allowing the ionization of the fast wind to change in response to this changing illumination means that the variability is enhanced over the range where the partially ionized material has most effect on the spectrum i.e. 0.7–2 keV (Gierliński & Done 2006). Fig. 8b shows how this does not produce enough enhancement of the variability to follow the sharp rise in rms at ~ 0.7 keV

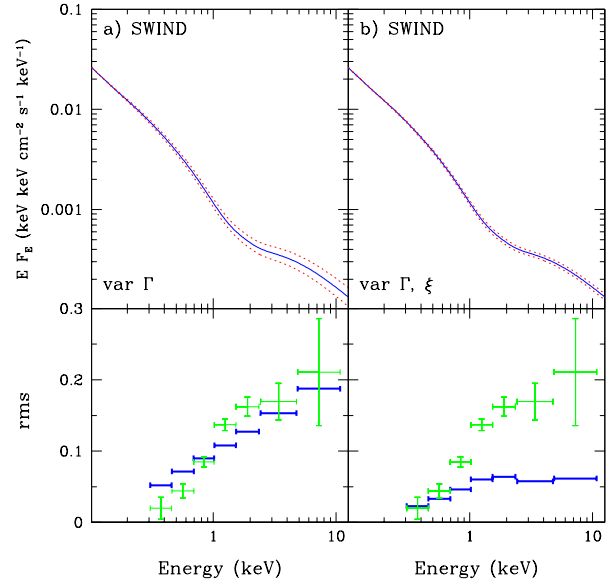


Figure 8. As for Fig. 4 but for a smeared absorption model for the soft excess. (a) shows the rms produced by pivoting the illuminating power law spectral index about the peak in seed photon flux at $3kT_{\text{seed}} \sim 0.15$ keV without changing the ionization of the absorber. Similarly to Fig. 6, this linear rise in rms as a function of energy does not match the sharper rise around 0.8 keV seen in the rapid variability. (b) shows that this low energy rise can be matched if the ionization responds to the changes in illumination as this enhances the variability over 0.7–2 keV where the absorption dominates. However, this also predicts that the variability drop above 2 keV, which is not seen in the data.

and it also predicts that this enhancement does not affect the spectrum above ~ 2 keV so the rms at high energies is also too small.

Thus while the smeared absorption model is a good fit to the spectrum, it cannot easily match the variability patterns seen, making it a less attractive solution.

4.4 Partial covering models: IONPCF1 and IONPCF2

If instead the absorption is clumpy then it can lead to clouds which partially cover the source. These can be ionized as they are illuminated by the central source, so we model this using partial covering by partially ionized material (ZXIPCF, available as an additional model for XSPEC). This fits the data fairly well (Fig. 9a) for a column with very low ionization covering 75 per cent of the source. We call this model IONPCF1. A second partially ionized, partial covering component is marginally significant ($\Delta\chi^2 = 12$ for 4 additional parameters), but this must be outflowing, with a blueshift of $0.12 \pm 0.01c$. This is similar to the velocities sometimes seen in highly ionized K α absorption lines from iron in high mass accretion rate AGN (e.g. the compilation Reeves et al. 2008), and also close to the theoretical expectations of the maximum velocity of a UV line driven disc wind (Proga et al. 2004). Hereafter we call this model IONPCF2.

Similarly to Fig. 6a and Fig. 8a, pivoting the power law at the peak flux of seed photons gives a linearly rising rms (Fig. 10a) which does not match the sharper rise in rms seen in the data. Again, dilution by a constant component at low energies is required, so Fig. 10b shows the variability pattern produced by assuming that the ionized absorption component at low energies remains constant while the rest of the spectrum varies as before.

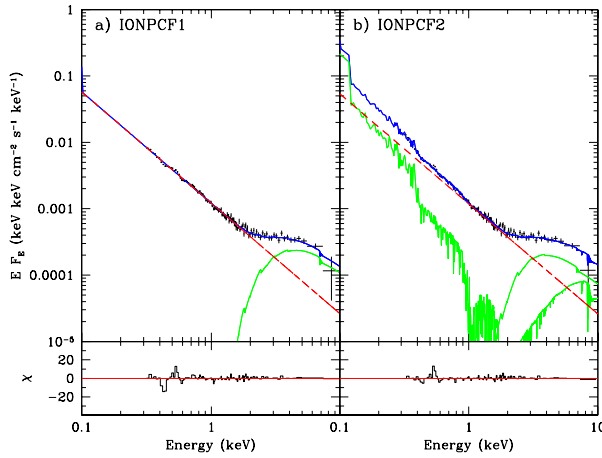


Figure 9. As for Fig. 3 but for a partial covering model for the soft excess. (a) has an intrinsically steep power law, part of which is strongly absorbed by nearly neutral material (light green curve) and part of which is unabsorbed (dashed red line). (b) shows a marginally better fit to the spectrum, where there is a second absorbed component from material which is ionized, so it also contributes at low energies.

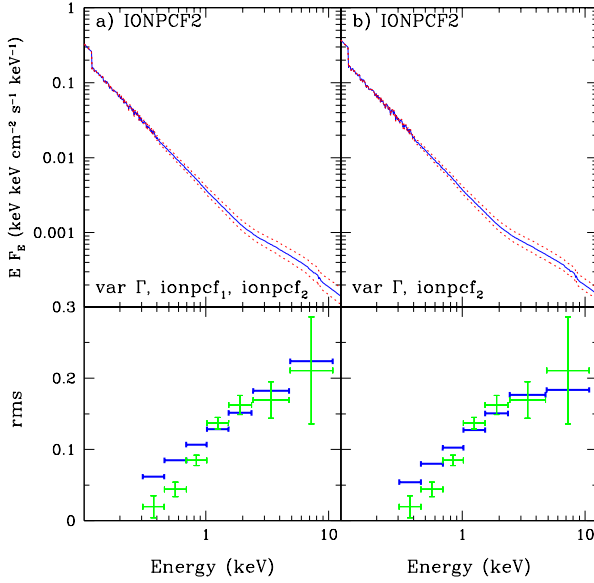


Figure 10. As for Fig. 4 but for the partial covering model for the soft excess. (a) shows the rms produced by pivoting the illuminating power law spectral index about the peak in seed photon flux at $3kT_{\text{seed}} \sim 0.15$ keV without changing the ionization of the absorber. Similarly to Fig. 6a and Fig. 8a, this linear rise in rms as a function of energy does not match the sharper rise around 0.8 keV seen in the rapid variability. (b) shows that this low energy rise is better fit if the ionized absorber which contributes at low energies is held constant while the power law pivots, but the model's predicted rise at ~ 0.8 keV is still stronger than is observed.

Model	Parameter	Value	$\chi^2_{\nu}/\text{d.o.f}$
COMP	Γ	$2.28^{+0.13}_{-0.10}$	289/210
	$N_{\text{PL}} (\times 10^{-4})$	$4.9^{+0.8}_{-0.3}$	
	kT_e (keV)	0.26 ± 0.03	
	N_{comptt}	$10.6^{+1.2}_{-0.8}$	
SWIND	Γ	$3.10^{+0.02}_{-0.05}$	306/210
	$N_{\text{PL}} (\times 10^{-4})$	$23.1^{+0.9}_{-0.7}$	
	$\lg \xi$	$2.82^{+0.09}_{-0.02}$	
	σ	$0.50^{+**}_{-0.05}$	
REF2	Γ	$3.61^{+0.08}_{-0.04}$	268/206
	$N_{\text{PL}} (\times 10^{-4})$	$9.4^{+0.3}_{-2.4}$	
	$\Omega_1/2\pi$	$0.43^{+1.05}_{-0.10}$	
	$R_{\text{in},1}$	$2.1^{+1.0}_{-0.8}$	
	$\lg \xi$	$3.02^{+0.16}_{-0.07}$	
	$\Omega_2/2\pi$	56^{+15}_{-18}	
	$R_{\text{in},2}$	$3.2^{+0.4}_{-1}$	
IONPCF1	Γ	3.69 ± 0.05	287/210
	$N_{\text{PL}} (\times 10^{-4})$	74 ± 13	
	$\lg \xi$	$0.8^{+0.3}_{-0.5}$	
	$N_H (10^{22} \text{ cm}^{-2})$	14^{+2}_{-3}	
	f	$0.84^{+0.02}_{-0.04}$	
IONPCF2	Γ	$3.68^{+0.09}_{-0.13}$	233/206
	$N_{\text{PL}} (\times 10^{-4})$	165^{+367}_{-69}	
	$\lg \xi_1$	$0.7^{+0.4}_{-0.9}$	
	$N_{H,1} (10^{22} \text{ cm}^{-2})$	12^{+2}_{-5}	
	f_1	0.80 ± 0.06	
	$\lg \xi_2$	$2.72^{+0.05}_{-0.5}$	
	$N_{H,2} (10^{22} \text{ cm}^{-2})$	153^{+13}_{-14}	
	f_2	$0.63^{+0.07}_{-0.09}$	
	v_2/c	0.12 ± 0.01	

Table 2. Best-fitting parameters of selected spectral models. Models described in the text that do not fit the spectrum are not shown here. Error bars are 90 per cent confidence, and $**$ denotes a parameter that reached its limit. Γ is the photon spectral index, N_{PL} is power-law normalization at 1 keV, ξ is the ionization (in the units of erg cm s^{-1}), σ is the velocity dispersion in the units of c , Ω is the reflector solid angle, R_{in} is the inner disc radius (in the units of GM/c^2), f is the covering factor.

Physically this could arise from light travel time delays if this is scattered from ionized material at some distance from the source. This produces some suppression of variability at low energies, but not as much as required to fit the rms of the rapid variability.

5 CONSTRAINTS FROM SPECTRA AND VARIABILITY

Any viable model for the soft excess must simultaneously fit both the spectrum and spectral variability with the same model parameters. The spectra alone can be fit with a variety of continua. There is clear curvature but this is degenerate. The spectra can either be fit with low energy spectral curvature, together with a ($\Gamma \sim 2.3$) power law at high energies, or with a steep power law at low energies ($\Gamma \sim 3.6$) together with curvature at high energies from emerging reflected (REF2) or absorbed components (IONPCF2), or by a somewhat less steep power law ($\Gamma \sim 3.3$) with curvature around 0.7–2 keV from absorption in a rapidly accelerating wind (SWIND). However, the energy dependence of the rapid X-ray variability (which is dominated by the QPO in these data)

Name	Description	XSPEC syntax
DISK	Standard disc	WABS(DISKBB+POWERLAW)
SLIM	Advection disc	WABS(DISKPB+POWERLAW)
COMP	Comptonized component	WABS(COMPTT+POWERLAW)
SWIND	Smeared wind absorption	WABS*SWIND(POWERLAW)
XSCORT	Ionized absorption/emission	WABS(XSCORT)
REF1	Ionized reflection (single)	WABS(POWERLAW+CONLINE*REFLBAL(POWERLAW))
REF2	Ionized reflection (double)	WABS(POWERLAW+CONLINE(THCOMP)+CONLINE*REFLBAL(POWERLAW))
IONPCF1	Single ionized partial covering	ZXIPCF*WABS(POWERLAW)
IONPCF2	Double ionized partial covering	ZXIPCF*ZXIPCF*WABS(POWERLAW)

Table 1. Summary of the models used in the paper.

breaks these degeneracies. The rms spectrum over the whole observation shows a smooth rise with energy, initially appearing to favour models where there is a single variable component (pivoting power law) which forms the spectrum. However, this rms is made up from two quite dissimilar variability patterns for the short and long timescales. Both these contain clear changes in the rms at ~ 0.7 keV, with the rapid variability amplitude strongly increasing with energy at this point while the longer timescale variability strongly decreases. These combine together in such a way as to produce an apparently featureless overall rms.

The rms of the rapid variability clearly supports the spectral decomposition where the soft excess is a separate, low temperature Comptonization component (COMP). The variability drops just where the low temperature Compton component starts to dominate, so the rms shape is easily produced from models where the soft excess remains constant and simply dilutes the variability of a high energy power law tail. This is very similar to the sorts of spectral decompositions used in binary systems, where the QPO (and all other rapid variability) is associated with the tail, not with the disc.

By contrast, the alternative spectral models (where the soft excess is an artifact of some distortion on an intrinsic steep power law spectrum) have much more difficulty in matching the energy dependence of the rapid variability. Pivoting the steep intrinsic power law at the peak energy of the seed photons gives a linearly rising rms, so some additional assumptions are required to produce the observed faster drop in variability at low energies. Changing the ionization of the absorber in the smeared wind model (SWIND) gives enhanced variability in the 0.7–2 keV region which matches well to the shape of the rms at low energies. However, this then drops above 2 keV where ionization changes no longer affect the spectrum, which does not match the observed rms.

By contrast, both the double reflector (REF2) and double partial covering model (IONPCF2) have ionized components at low energies, so holding these constant while the rest of the spectrum responds to the pivoting power law dilutes the low energy variability. However, physically this seems somewhat contrived, and both these (but especially IONPCF2) have difficulties in suppressing enough variability at the lowest energies.

Thus the combined spectral and spectral variability constraints strongly favour the model where the soft excess is a true continuum component, described by a low temperature Comptonized disc component (COMP). The long timescale variability can also be explained in this spectral decomposition by changing the temperature and/or optical depth of the Comptonization to give a predicted rms which matches the data very well. However, the light curve shows that there can also be discrete energy dependent events (the dip), which seems more likely to be from an occultation. If so, then there

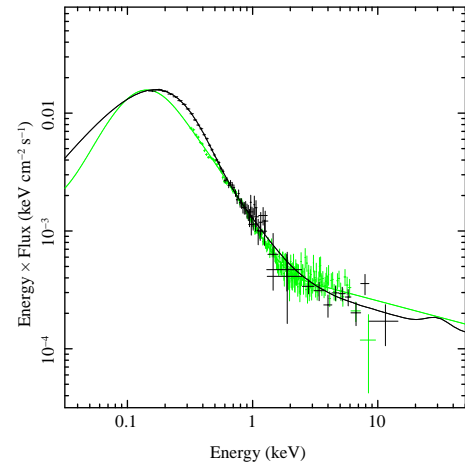


Figure 11. Comparison of RE J1034+396 (light green) and GRS 1915+105 (black) energy spectra. Both spectra are unfolded and unabsorbed using the best-fitting model. The GRS 1915+105 spectrum was shifted in energy by factor 20 and renormalized to match the RE J1034+396 spectrum.

should also be some contribution from absorption in the spectrum, and this might also shape the longer timescale variability.

6 CONSTRAINTS FROM THE BROAD BAND SPECTRAL ENERGY DISTRIBUTION

This decomposition of the X-ray spectrum into a Comptonized disc with separate tail to high energies (COMP) also looks sensible in the light of the overall spectral energy distribution. Both the UV/EUV/soft X-ray shape and the rms variability of the X-ray emission show that this peaks at ~ 0.15 keV (Puchnarewicz et al. 2000; Casebeer et al. 2006; Fig. 2). Integrating the COMP model down to this energy gives a luminosity of $\sim 7 \times 10^{43}$ ergs s^{-1} . This is already more than 10 per cent of the bolometric luminosity of $\sim 5 \times 10^{44}$ ergs s^{-1} . However, in the reflection and partial covering models, REF2 and IONPCF2, the observed soft X-ray flux is only a small fraction of the total illuminating power law. The hidden emission required by both these models is a factor ~ 10 larger. This luminosity must be reprocessed, yet is more than the total bolometric luminosity of the source! Thus these two models fail on energetics as well as requiring somewhat contrived assumptions in order to match the rms variability and requiring an uncomfortably steep ($\Gamma \sim 3.6$) intrinsic continuum.

This all strongly supports the conclusion that in RE J1034+396 the soft excess is a Comptonized disc com-

ponent, connecting smoothly onto the EUV peak of the spectral energy distribution and extending out to ~ 1 keV. This does not have an obvious counterpart in the typical black hole binary systems. These can show convincingly clean disc spectra (thermal dominant state, high/soft state, ultrasoft state), or higher temperature Comptonization (10–20 keV: very high state, intermediate state, steep power law state), but generally they do not show low temperature Comptonization (see e.g. Done, Gierliński & Kubota 2007). However, most of these systems have $L/L_{\text{Edd}} < 1$, so they may not be a good guide to the spectra of super Eddington flows. The disc structure should change at such high mass accretion rates, with strong winds potentially increasing the amount of material in the corona, leading to mass loading of the acceleration mechanism and decreasing energy per particle. Whatever the origin, a similar process of low temperature disc Comptonization probably happens in the unique galactic black hole binary GRS 1915+105. This is the only black hole binary in our Galaxy which consistently shows super Eddington luminosities (Done, Wardziński & Gierliński 2004), and it can show spectra which are dominated by a huge, low temperature Comptonized disc component, with a weak power law tail to higher energies. Fig. 11 shows how one of these spectra from GRS 1915+105 (the low ω state in fig. 7 of Zdziarski et al. 2005) fits almost exactly onto the XMM-Newton spectrum of RE J1034+396 with a shift in energy scale by a factor 20. This gives a mass estimate for RE J1034+396 of $\sim 2 \times 10^6 M_{\odot}$ from scaling the disc temperature as $M^{-1/4}$, which seems quite reasonable (Puchnarewicz et al. 2002).

Understanding the origin of the soft excess in RE J1034+396 may not necessarily solve the problem of the soft excess in general. The spectral energy distribution of this object is plainly rather different from that in most other high mass accretion rate AGN in that the soft excess contains a large fraction of the bolometric luminosity of the source (Middleton et al. 2007). Spectral distortion models (reflection or absorption) are clearly more likely to explain a feature carrying only a small fraction of the bolometric luminosity. Instead, the continuous EUV/soft X-ray excess in RE J1034+396 clearly favours a common origin for the disc and soft excess, unlike that for most other quasars, where the UV and soft X-rays do not appear to smoothly connect to each other in individual objects (Haro-Corzo et al. 2007).

7 CONCLUSIONS

The combined constraints from the spectrum and variability show the soft excess in RE J1034+396 is most likely a smooth extension of the accretion disc peak in the EUV probably arising from low temperature Comptonization of the disc. This remains more or less constant on short timescales, diluting the QPO and rapid variability seen in the power law tail at the low energies where the soft excess dominates. As in the black hole binary systems, the QPO is a feature of the tail *not* of the disc.

The conclusion that the soft excess is a low temperature Comptonization of the disc emission may not necessarily be more widely applicable to other NLS1. The spectrum of RE J1034+396 is unique, so extrapolating results from this object may not be justified. In particular, if this object has a very high (super Eddington?) mass accretion rate then it could enter a new accretion state (perhaps analogous to the unique galactic binary GRS 1915+105 and the Ultra Luminous X-ray sources: Roberts 2008) which may also be the trigger for its so far unique QPO. A different origin for the soft excess in RE J1034+396 has the advantage that it would not

require some unknown physical mechanism to restrict the temperature of the continuum in all objects to a narrow range (Gierliński & Done 2004), though does require a coincidence that this temperature in RE J1034+396 is so close to that ubiquitously seen for the soft excess. Nonetheless, it is clearly possible that in selecting the most extreme soft excess object, we have also selected the one where the the soft excess has a different origin.

REFERENCES

Abramowicz M. A., Czerny B., Lasota J. P., Szuszkiewicz E., 1988, *ApJ*, 332, 646
 Ballantyne D. R., Iwasawa K., Fabian A. C., 2001, *MNRAS*, 323, 506
 Bechtold J., Czerny B., Elvis M., Fabbiano G., Green R. F., 1987, *ApJ*, 314, 699
 Boller T., Brandt W. N., Fink H., 1996, *A&A*, 305, 53
 Boroson T. A., 2002, *ApJ*, 565, 78
 Brandt W. N., Mathur S., Elvis M., 1997, *MNRAS*, 285, L25
 Brocksopp C., Starling R. L. C., Schady P., Mason K. O., Romero-Colmenero E., Puchnarewicz E. M., 2006, *MNRAS*, 366, 953
 Casebeer D. A., Leighly K. M., Baron E., 2006, *ApJ*, 637, 157
 Chevallier L., Collin S., Dumont A.-M., Czerny B., Mouchet M., Gonçalves A. C., Goosmann R., 2006, *A&A*, 449, 493
 Churazov E., Forman W., Jones C., Böhringer H., 2000, *A&A*, 356, 788
 Crummy J., Fabian A. C., Gallo L., Ross R. R., 2006, *MNRAS*, 365, 1067
 Czerny B., Elvis M., 1987, *ApJ*, 321, 305
 Czerny B., Niłakajuk M., Różańska A., Dumont A.-M., Loska Z., Źycki P. T., 2003, *A&A*, 412, 317
 D'Ammando F., Bianchi S., Jiménez-Bailón E., Matt G., 2008, *A&A*, 482, 499
 Dewangan G. C., Griffiths R. E., Dasgupta S., Rao A. R., 2007, *ApJ*, 671, 1284
 Done C., 2007, *PThPS*, 169, 248
 Done C., Gierliński M., 2005, *MNRAS*, 364, 208
 Done C., Gierliński M., 2006, *MNRAS*, 367, 659
 Done C., Nayakshin S., 2007, *MNRAS*, 377, L59
 Done C., Gierliński M., Kubota A., 2007, *A&ARv*, 15, 1
 Done C., Wardziński G., Gierliński M., 2004, *MNRAS*, 349, 393
 Edelson R., Turner T. J., Pounds K., Vaughan S., Markowitz A., Marshall H., Dobbie P., Warwick R., 2002, *ApJ*, 568, 610
 Fabian A. C., Ballantyne D. R., Merloni A., Vaughan S., Iwasawa K., Boller T., 2002, *MNRAS*, 331, L3
 Fabian A. C., Miniutti G., Gallo L., Boller T., Tanaka Y., Vaughan S., Ross R. R., 2004, *MNRAS*, 353, 1071
 Fukue J., 1996, *PASJ*, 48, 631
 Gallo L. C., Boller T., Tanaka Y., Fabian A. C., Brandt W. N., Welsh W. F., Anabuki N., Haba Y., 2004, *MNRAS*, 347, 269
 Gallo L. C., Brandt W. N., Costantini E., Fabian A. C., 2007, *MNRAS*, 377, 1375
 Gierliński M., Done C., 2004, *MNRAS*, 349, L7
 Gierliński M., Zdziarski A. A., 2005, *MNRAS*, 363, 1349
 Gierliński M., Done C., 2006, *MNRAS*, 371, L16
 Gierliński M., Middleton M., Ward M., Done C., 2008, *Natur*, in press (arXiv:0807.1899)
 Haba Y., Terashima Y., Kunieda H., Ohsuga K., 2008, *PASJ*, 60, 487
 Haro-Corzo S. A. R., Binette L., Krongold Y., Benitez E., Humphrey A., Nicastro F., Rodríguez-Martínez M., 2007, *ApJ*, 662, 145
 Kawaguchi T., 2003, *ApJ*, 593, 69
 Laor A., 1991, *ApJ*, 376, 90
 Larsson J., Miniutti G., Fabian A. C., Miller J. M., Reynolds C. S., Ponti G., 2008, *MNRAS*, 384, 1316
 Leighly K. M., 1999, *ApJS*, 125, 317
 Leighly K. M., 2005, *Ap&SS*, 300, 137
 Malzac J., Dumont A. M., Mouchet M., 2005, *A&A*, 430, 761
 Maoz D., 2007, *MNRAS*, 377, 1696
 Markowitz A., Edelson R., Vaughan S., 2003, *ApJ*, 598, 935

McClintock J. E., Remillard R. A., 2006, in: Compact stellar X-ray sources. W. Lewin, M. van der Klis (Eds.). Cambridge Astrophysics Series, No. 39, Cambridge University Press, 157

M^cHardy I. M., Koerding E., Knigge C., Uttley P., Fender R. P., 2006, *Natur*, 444, 730

McKernan B., Yaqoob T., 1998, *ApJ*, 501, L29

Middleton M., Done C., Gierliński M., 2007, *MNRAS*, 381, 1426

Middleton M., Done C., Schurch N., 2008, *MNRAS*, 383, 1501

Miller L., Turner T. J., Reeves J. N., George I. M., Kraemer S. B., Wingert B., 2007, *A&A*, 463, 131

Miller L., Turner T. J., Reeves J. N., 2008, *A&A*, 483, 437

Miniutti G., Fabian A. C., 2004, *MNRAS*, 349, 1435

Mineshige S., Kawaguchi T., Takeuchi M., Hayashida K., 2000, *PASJ*, 52, 499

Murashima M., Kubota A., Makishima K., Kokubun M., Hong S., Negoro H., 2005, *PASJ*, 57, 279

O'Neill P. M., Nandra K., Cappi M., Longinotti A. L., Sim S. A., 2007, *MNRAS*, 381, L94

Ponti G., Miniutti G., Cappi M., Maraschi L., Fabian A. C., Iwasawa K., 2006, *MNRAS*, 368, 903

Pounds K. A., Done C., Osborne J. P., 1995, *MNRAS*, 277, L5

Proga D., Kallman T. R., 2004, *ApJ*, 616, 688

Puchnarewicz E. M., Mason K. O., Siemiginowska A., Fruscione A., Comastri A., Fiore F., Cagnoni I., 2001, *ApJ*, 550, 644

Reeves J., Done C., Pounds K., Terashima Y., Hayashida K., Anabuki N., Uchino M., Turner M., 2008, *MNRAS*, 385, L108

Risaliti G., Elvis M., Fabbiano G., Baldi A., Zezas A., Salvati M., 2007, *ApJ*, 659, L111

Roberts T. P., 2008, Proc. ESAC faculty workshop on X-rays from nearby galaxies, MPE Report 295, 42

Ross R. R., Fabian A. C., Ballantyne D. R., 2002, *MNRAS*, 336, 315

Shemmer O., Brandt W. N., Netzer H., Maiolino R., Kaspi S., 2006, *ApJ*, 646, L29

Schurch N. J., Done C., 2006, *MNRAS*, 371, 81

Schurch N. J., Done C., 2007, *MNRAS*, 381, 1413

Schurch N. J., Done C., 2008, *MNRAS*, 386, L1

Sobolewska M. A., Done C., 2007, *MNRAS*, 374, 150

Tanaka Y., Boller T., Gallo L., Keil R., Ueda Y., 2004, *PASJ*, 56, L9

Turner T. J., Reeves J. N., Kraemer S. B., Miller L., 2008, *A&A*, 483, 161

van der Klis M., 2005, *AN*, 326, 798

Vaughan S., Fabian A. C., 2004, *MNRAS*, 348, 1415

Vaughan S., Uttley P., 2005, *MNRAS*, 362, 235

Vaughan S., Edelson R., Warwick R. S., Uttley P., 2003, *MNRAS*, 345, 1271

Wang J.-M., Netzer H., 2003, *A&A*, 398, 927

Watarai K.-y., Fukue J., Takeuchi M., Mineshige S., 2000, *PASJ*, 52, 133

Yuan W., Zhou H. Y., Komossa S., Dong X. B., Wang T. G., Lu H. L., Bai J. M., 2008, arXiv, 806, arXiv:0806.3755

Zdziarski A. A., Gierliński M., Rao A. R., Vadawale S. V., Mikołajewska J., 2005, *MNRAS*, 360, 825

Życki P. T., Done C., Smith D. A., 2001, *MNRAS*, 326, 1367